Global-scale mapping of changes in ecosystem functioning from earth observation-based trends in total and recurrent vegetation

Fensholt, Rasmus; Horion, Stéphanie; Tagesson, Torbern; Ehammer, Andrea; Ivits, Eva; Rasmussen, Kjeld

Published in:
Global Ecology and Biogeography

DOI:
10.1111/geb.12338

2015

Document Version:
Publisher's PDF, also known as Version of record

A Journal of Macroecology

Global Ecology and Biogeography

RESEARCH PAPER

Global-scale mapping of changes in ecosystem functioning from earth observation-based trends in total and recurrent vegetation

Rasmus Fensholt[1]*, Stéphanie Horion[1], Torbern Tagesson[1], Andrea Ehammer[1], Eva Ivits[2] and Kjeld Rasmussen[1]

[1]*Department of Geosciences and Natural Resource Management, University of Copenhagen, DK-1350 Copenhagen, Denmark,* [2]*Ecosystems Assessment, European Environment Agency, DK-1050 Copenhagen, Denmark*

*Correspondence: Rasmus Fensholt, Department of Geosciences and Natural Resource Management, University of Copenhagen, Øster Voldgade 10, DK-1350 Copenhagen, Denmark.
E-mail: rf@ign.ku.dk

ABSTRACT

Aim To evaluate trend analysis of earth observation (EO) dense time series as a new way of describing and mapping changes in ecosystem functioning at regional to global scales. Spatio-temporal patterns of change covering 1982–2011 are discussed in the context of changes in land use and land cover (LULCC).

Location Global.

Methods This study takes advantage of the different phenological cycles of recurrent vegetation (herbaceous vegetation) and persistent vegetation (woody/shrub cover) in combining trend analyses of global-scale vegetation based on different annual/seasonal normalized difference vegetation index (NDVI) metrics. Spatial patterns of combined vegetation trends derived from the Global Inventory Modeling and Mapping Studies NDVI are analysed using land-cover information (GLC2000).

Results The direction of change in annual and seasonal NDVI metrics is similar for most global terrestrial ecosystems, but areas of diverging trends were also observed for certain regions across the globe. These areas are shown to be dominated by land-cover classes of deciduous forest in tropical/subtropical areas. Areas of observed change are found in dry deciduous forest in South America and central southern Africa and are in accordance with studies of hotspot LULCC areas conducted at local and regional scales. The results show that dense time series of EO data can be used to map large-scale changes in ecosystem functional type that are due to forest cover dynamics, including forest degradation, deforestation/reforestation and bush encroachment.

Main conclusions We show that areas characterized by changes in ecosystem functioning governed by LULCC at regional and global scales can be mapped from dense time series of global EO data. The patterns of diverging NDVI metric trends can be used as a reference in evaluating the impacts of environmental changes related to LULCC and the approach may be used to detect changes in ecosystem functioning over time.

Keywords

Ecosystem functioning change, land-use land-cover change (LULCC), remote sensing, vegetation greenness, phenology, trend analysis.

DOI: 10.1111/geb.12338
http://wileyonlinelibrary.com/journal/geb

INTRODUCTION

Plant functional types (PFTs) are characterized by the physiognomy and functional dynamics of the vegetation. PFTs summarize the complexity of individual species and populations in recurrent patterns of plants that exhibit similar responses to biophysical environmental conditions. Hence, PFTs bridge the spatial and functional gaps between plant physiology, the biophysical properties of the land and ecosystem processes (Paruelo *et al*., 2001). In recent decades the concept of ecosystem functional types (EFTs) has been developed for the global-scale assessment of ecosystems based on the concept of PFTs (Alcaraz-Segura *et al*., 2006). EFTs have been applied in a wide sense for areas characterized by similar ecological attributes, such as PFT composition, structure, phenology, biomass or productivity (Scholes *et al*., 1997). Earth observation (EO)-based mapping of changes in ecosystems provides a powerful tool for global change research that assesses the impact of land use and climate modifications (Ivits *et al*., 2013, 2014). Human activities, along with climate change, are known to influence the local structural properties and productivity of ecosystems, but large-scale assessment of the distribution of such changes is difficult using conventional EO methods. Traditionally, deforestation has been monitored successfully from high-resolution imagery like Landsat (Asner *et al*., 2009; Hansen *et al*., 2013). However, large-scale changes from forest degradation are more challenging to monitor using EO data (Lambin, 1999; Joseph *et al*., 2011) and standard approaches based on binary classifications risk oversimplifying the effects of degradation.

Time series of continuous EO-based estimates of vegetation have significantly improved our understanding of inter-annual changes in vegetation from a regional to a global scale (Nemani *et al*., 2003; de Jong *et al*., 2011). The normalized difference vegetation index (NDVI) (Tucker, 1979) has been found to be related to vegetation greenness or vigour (Myneni *et al*., 1995) and is widely used as a proxy for the distribution of net primary production (NPP) due to the availability of data covering more than three decades from the early 1980s until the present. Analysis of trends in vegetation productivity and their drivers at global and regional scales is done in different ways depending on the biome studied: EO-based vegetation sums/averages over the full year (Fensholt *et al*., 2012; van Leeuwen *et al*., 2013; An *et al*., 2014) or seasonal integrals ($NDVI_{SIN}$) based on specific months covering the growing season (Piao *et al*., 2006; Fensholt *et al*., 2013) are widely used. However, the choice of vegetation integration method and period (annual or seasonal) has implications for the analysis of long-term NDVI trends. We suggest that the vegetation parameterization methods should be seen in the context of the structural attributes of ecosystems, such as vegetation physiognomy or the composition of PFTs to improve the understanding of changes in ecosystem function. Recurrent vegetation comprises species that operate in (often annual) cycles of activity and dormancy (Donohue *et al*., 2009), and $NDVI_{SIN}$ captures the combined contributions of deciduous, annual and ephemeral species. Trend estimates based on different NDVI metrics might thus reveal different or complementary information on changes in recurrent and total vegetation cover. An analysis combining different NDVI metric trends is thereby expected to reveal information on gradually occurring changes in structural or functional attributes of ecosystems related to processes of forest degradation and woody/shrub encroachment.

This study combines global-scale trend analysis based on two different NDVI metrics [annual mean NDVI values ($NDVI_{mean}$) and growing season integrals of NDVI ($NDVI_{SIN}$)] from the Global Inventory Modeling and Mapping Studies (GIMMS) dataset for a 30-year period (1982–2011). Areas of diverging trends in NDVI metrics are analysed as a function of land-use cover at regional and continental scales and spatio-temporal patterns are discussed in relation to well-known changes in land use and land cover (LULCC).

MATERIALS AND METHODS

Annual changes in any NDVI metric will be caused by changes in either the NDVI amplitude (photosynthetic vigour) or frequency (season length/timing), or a combination of the two (Fig. S1 in Supporting Information). Amplitude changes can be described by changes in either the seasonal low value (increase/decrease/constant) or the seasonal high value (increase/decrease/constant), yielding nine different combinations, of which three can potentially generate constant amplitude (in the case of no shift/equal shift in high/low value). Changes in frequency can also be described by nine different combinations of an earlier/later/constant start/end of the growing season, of which three can produce a constant season length (in the case of no shift/equal shift in start/end value). This leads to a total of 81 different combinations of constant/increasing/decreasing (for low/high values) seasonal amplitude and earlier/later/constant (for start/end values) seasonal frequency. Numerical analysis of the 81 different combinations of changing amplitude/frequency showed that only cases involving an amplitude change caused by a change in the seasonal low value are able to produce a divergence between integral size of the seasonal sum of $NDVI_{mean}$ and $NDVI_{SIN}$.

The GIMMS 15-day composite NDVI product (GIMMS3g)

For this study the newly released third-generation GIMMS NDVI data covering the period 1982 to 2011 (bi-monthly GIMMS3g NDVI provided in 1/12° resolution; Pinzon & Tucker, 2014) were used.

The MOD10CM Moderate Resolution Imaging Spectroradiometer snow-cover product

Global snow extent (maximum snow cover) is provided by the Moderate Resolution Imaging Spectroradiometer (MODIS) MOD10CM snow-cover product on a monthly basis at a 0.05° spatial resolution. For this study, the monthly MOD10CM global data from 2000 to 2012 were used.

Global land-cover data

Global land-cover classes (GLC2000; Bartholomé *et al.*, 2002) are based on the SPOT-4 VEGETATION VGT2000 dataset provided by the Centre National d'Études Spatiales (CNES) and the land-cover classification system provided by Food and Agriculture Organization of the United Nations (FAO; Di Gregorio & Jansen, 2000). GLC2000 defines the boundaries of the different ecosystems such as forest, herbaceous and cultivated systems. GLC2000 land-cover classes are used here but are also merged into more general vegetation categories related to ecosystem functioning (referred to here as EFTs).

Estimation of NDVI metrics

Two different NDVI metrics were used in this study: $NDVI_{mean}$ and $NDVI_{SIN}$. $NDVI_{SIN}$ was computed from time series parameterization using a Savitsky–Golay filter available in the TIMESAT software (Jonsson & Eklundh, 2002, 2004). The Savitsky–Golay filter is a moving filter that fits values from a least squares fit to a polynomial (Jonsson & Eklundh, 2004). From the per-pixel polynomial fit the onset and end of the growing season are determined for individual years based on a parameterization of the fitted seasonal NDVI curve. The parameterization is based on percentage NDVI levels of the total seasonal NDVI amplitude. The integral representing the seasonally active vegetation is estimated by the area between the fitted function and the average level of the left and right minima. The following Savitsky–Golay fitting parameters were applied: seasonal parameter = 0.5; number of envelope iterations = 2; adaptation strength = 1; Savitzky–Golay window size = 2; amplitude season start and end = 20%.

Trend estimation

Linear temporal trend analysis was conducted to estimate the magnitude and direction of changes in $NDVI_{mean}$ and $NDVI_{SIN}$. Per-pixel trends were calculated by applying a nonparametric linear regression model with time as the independent variable and NDVI metrics as the dependent variable. The outputs of the trend analyses are maps of regression slope values, indicating the strength and magnitude of the calculated trend. Since time series of NDVI often do not meet parametric assumptions of normality and homoscedasticity (Hirsch & Slack, 1984) a median trend (Theil–Sen, TS) procedure was applied (Hoaglin *et al.*, 2000), as suggested for studies of vegetation trends based on time series of NDVI data (de Beurs & Henebry, 2005). The TS procedure is furthermore resistant to outliers and therefore suitable for assessing the rate of change in short or noisy series (Eastman *et al.*, 2009). The significance of $NDVI_{mean}$ and $NDVI_{SIN}$ time series trends was calculated by the nonparametric Mann–Kendall (MK) significance test. The MK significance test is commonly used as a trend test for the TS median slope operator (Eastman *et al.*, 2009) and produces outputs of *z*-scores that allow for the assessment of both the significance and direction of the trend.

Trend difference map

Significance maps (*z*-scores) of $NDVI_{mean}$ and $NDVI_{SIN}$ time series trends were reclassified into seven classes: positive/negative trends at confidence levels of 90% ($P < 0.1$), 95% ($P < 0.05$) and 99% ($P < 0.01$) and not significant ($P > 0.1$) (Fig. 1a, b). These maps were combined into a single trend difference map by aggregating all significant positive and negative trends, respectively, to a single class covering pixels that are significant at the 90% level ($P < 0.1$) (one for positive and one for negative trends) before being combined, yielding seven possible combinations (Fig. 2 and a–g in Table S1). A significance level of 90% was chosen to maintain the clearest possible pattern of regional-scale clusters of pixels characterized by different trend combinations.

Masking based on methodological constraints

Calculation of $NDVI_{SIN}$ requires seasonality to be present in the vegetation for the EO-based signal in order to achieve robust curve fitting. Pixels with an annual NDVI standard deviation (SD) of < 0.02 were masked as this threshold was found to be appropriate for delineating areas without vegetation activity (Fensholt & Proud, 2012). Also, some areas of tropical broadleaved evergreen forest are characterized by a seasonality that is too limited for a robust calculation of $NDVI_{SIN}$, and these areas were masked from the combined criteria of both low NDVI SD (< 0.075) and high annual mean NDVI (> 0.7).

Temporal trends in annual mean NDVI ($NDVI_{mean}$) can potentially be influenced by changes/trends in snow cover. Therefore a combined mask was produced from a two-step analysis using the GIMMS quality flags (1982–2011) and MODIS snow-cover extent data (2000–12). In Step 1 pixels that were covered by snow for at least 1 month a year (average value for 2000–12) were masked, as were (in Step 2) pixels for which a significant trend in GIMMS flag values indicated an influence of snow cover (1982–2011).

Different masks were applied for the individual analyses of NDVI metrics ($NDVI_{SIN}$ and $NDVI_{mean}$) to preserve the maximum spatial output extent of pixels produced by each method (Fig. 1a, b). A direct comparison of trends from $NDVI_{mean}$ and $NDVI_{SIN}$ (Figs 2–5) was made for the common denominator of non-masked pixels.

RESULTS

Trends in $NDVI_{mean}$ and $NDVI_{SIN}$

Significant linear trends in annual mean GIMMS NDVI ($NDVI_{mean}$) 1982–2011 (Fig. 1a) cover 48.9% of the pixels that were not masked ($n = 1{,}166{,}866$) (35% by significantly positive trends and 13.9% by significantly negative trends; $P < 0.1$). Large areas of negative trends can be found in the arid areas of the Sahara, the Middle East and north-west China. Also, large areas in South America (Argentina and Paraguay) and in Africa, cross-continentally along 15° S (Angola, Zimbabwe,

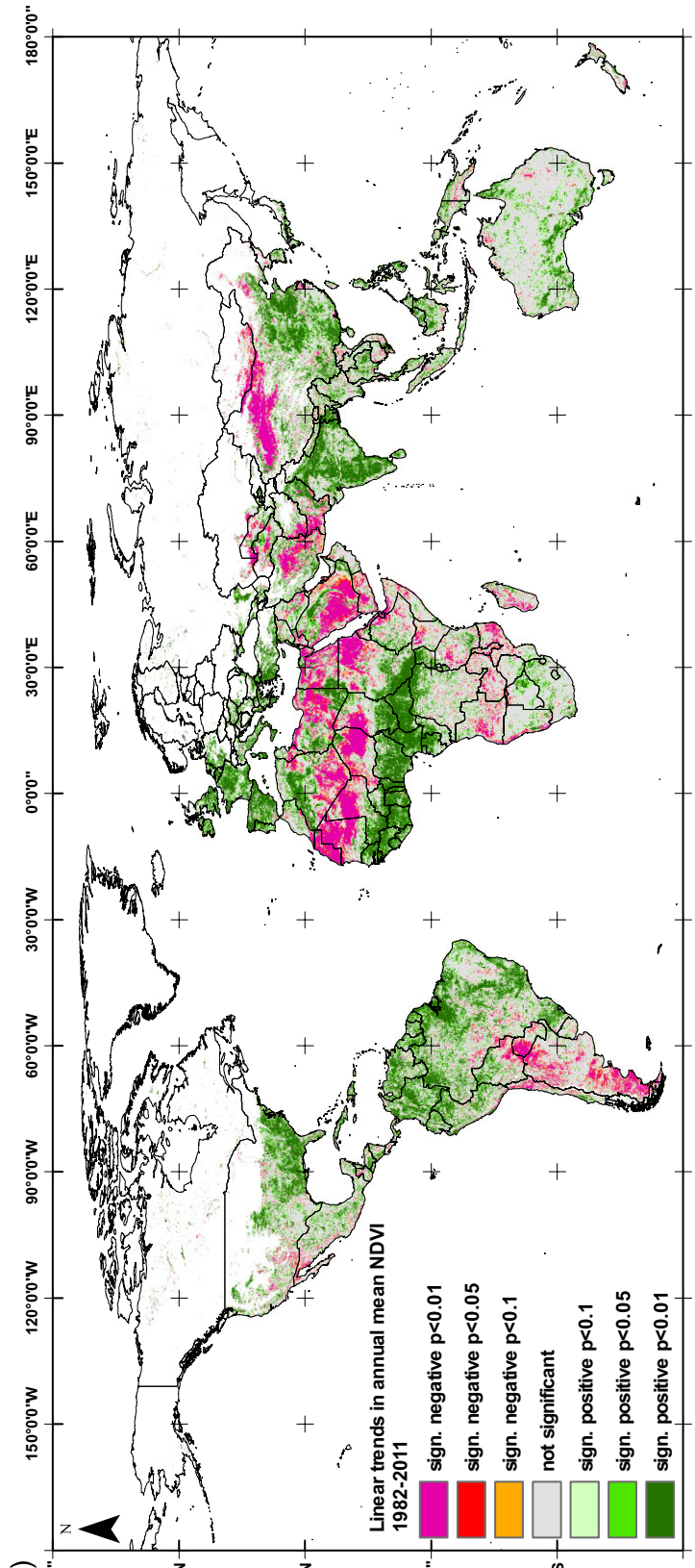

Figure 1 (a) Linear trends in annual mean vegetation greenness ($NDVI_{mean}$) 1982–2011 [areas influenced by snow cover have been masked (white)]. (b) Linear trends in growing season integrated vegetation greenness ($NDVI_{SIN}$) 1982–2011 [areas not suitable for growing season integration have been masked (white)].

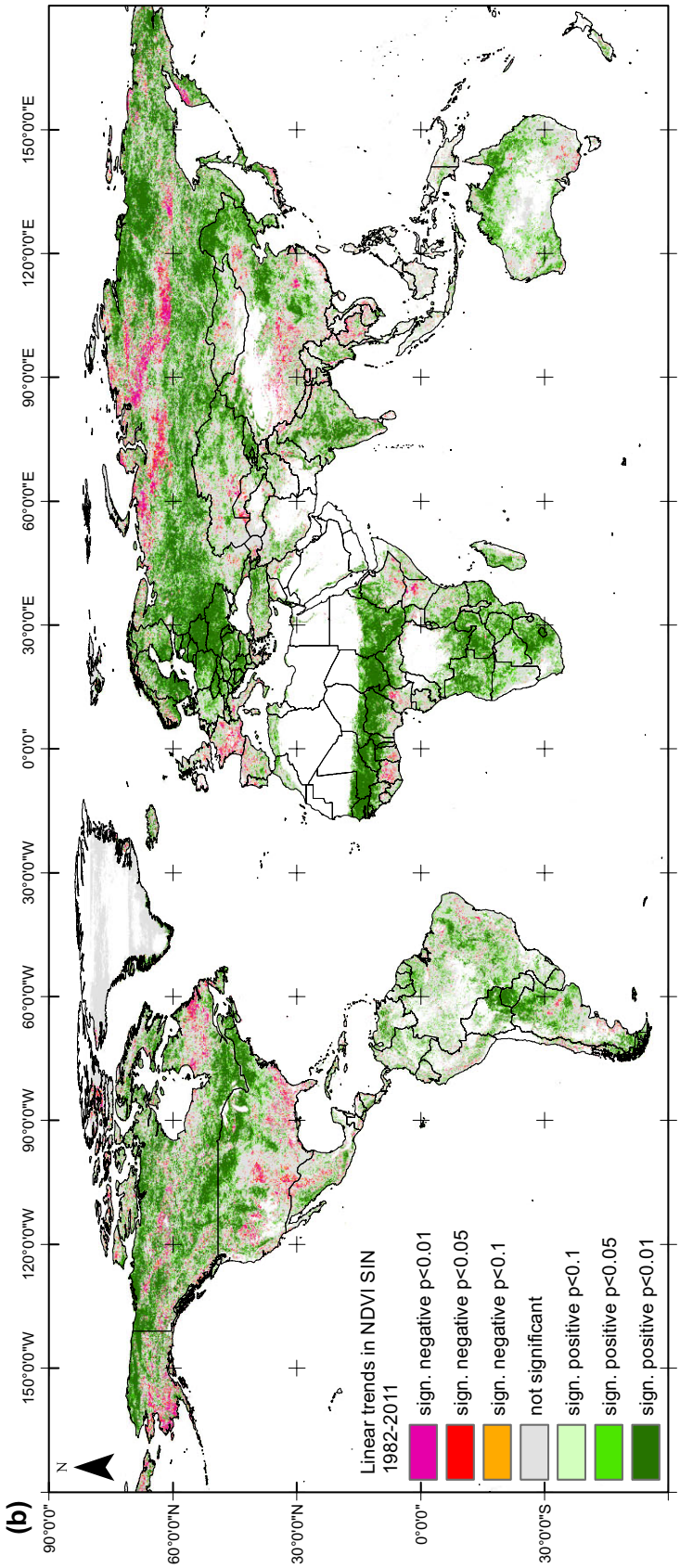

Figure 1 *Continued*

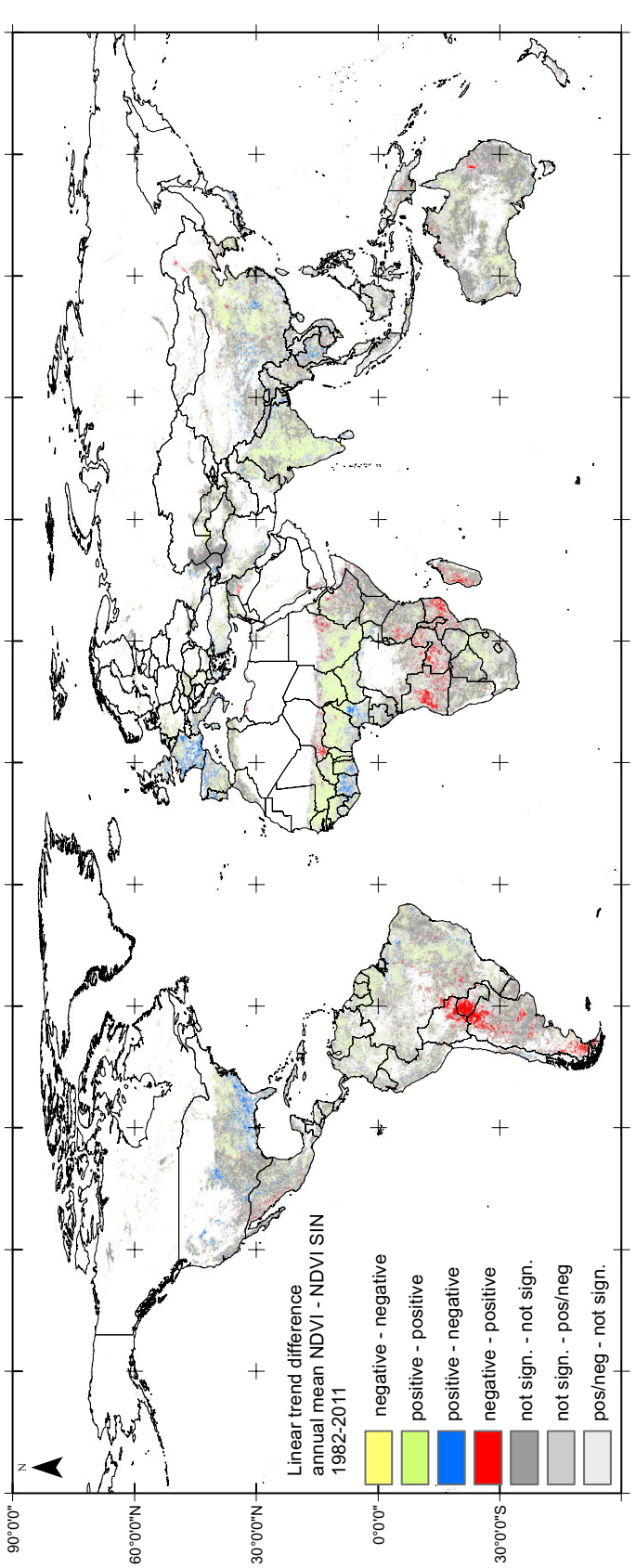

Figure 2 Trend differences in annual mean and growing season integrated vegetation greenness ($NDVI_{mean}$–$NDVI_{SIN}$ 1982–2011) [areas influenced by snow cover and areas not suitable for growing season integration have been masked (white)].

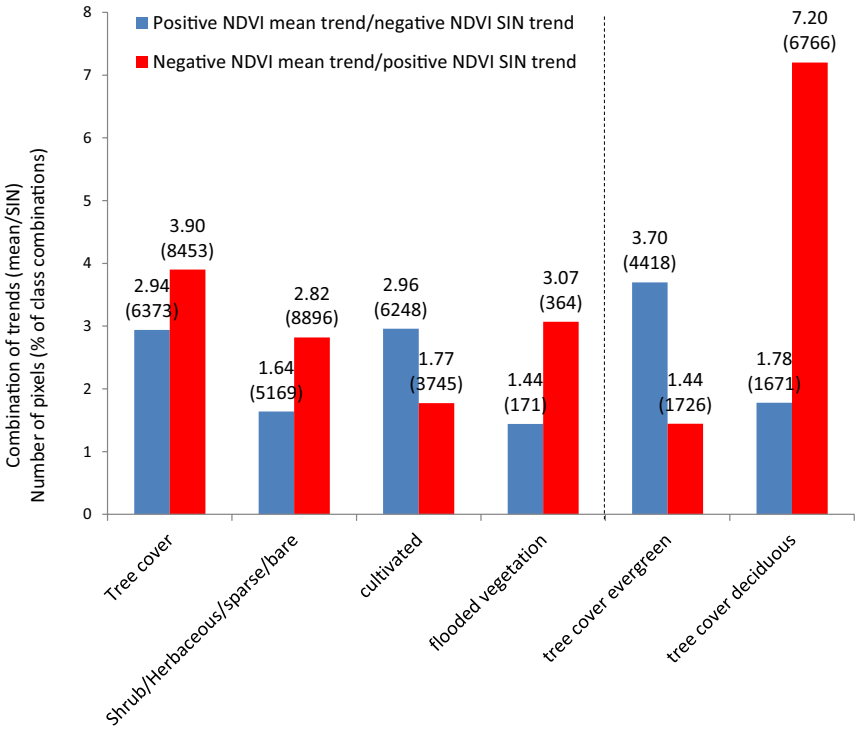

Figure 3 Number of pixels (in per cent) of diverging trends ('diverging trends case 1' and 'diverging trends case 2'; Table S1) for different ecosystem functional types (number of pixel counts are given in parentheses). On the right side of the figure tree cover is subdivided into evergreen and deciduous.

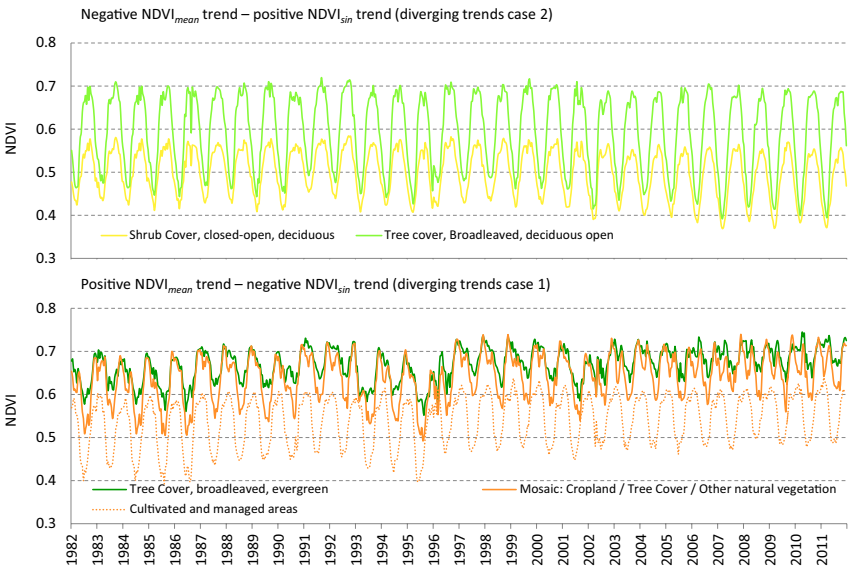

Figure 4 Time series of vegetation greenness (15-day composite GIMMS3g NDVI) for pixels characterized by diverging trends: 'diverging trends case 2' (top) and 'diverging trends case 1' (bottom) for different land-cover classes [deciduous shrub and tree cover (top) and evergreen tree cover and cropland/cultivated areas (bottom)].

Mozambique, and Madagascar), are characterized by significant negative trends in annual mean GIMMS NDVI. Large regions of significant positive $NDVI_{mean}$ trends can be seen in western Europe, the Mediterranean region, India, south-west China, Sahelian and Guinean Africa, south-east USA and northern and central South America. For Australia, a lower percentage of significant pixels can be observed, the majority of them positive.

The analysis of trends of growing season integrated NDVI ($NDVI_{SIN}$) for 1982–2011 (Fig. 1b) covers a much larger spatial extent (n = 3,089,545 pixels) since the growing season integral of vegetation in areas influenced by snow cover can still be analysed using the $NDVI_{SIN}$ approach (Fensholt & Proud, 2012). Of the pixels that are not masked, 33.6% show a significant trend (29.0% and 4.6% being significantly positive and negative, respectively). For areas where both NDVI metrics can be derived, large regions in the Southern Hemisphere (South America and in Africa, cross-continentally along 15° S) show significant positive trends in $NDVI_{SIN}$ but significant negative trends in $NDVI_{mean}$, whereas the opposite pattern is visible for areas in south-east USA, western Europe, Guinean Africa and Southeast Asia.

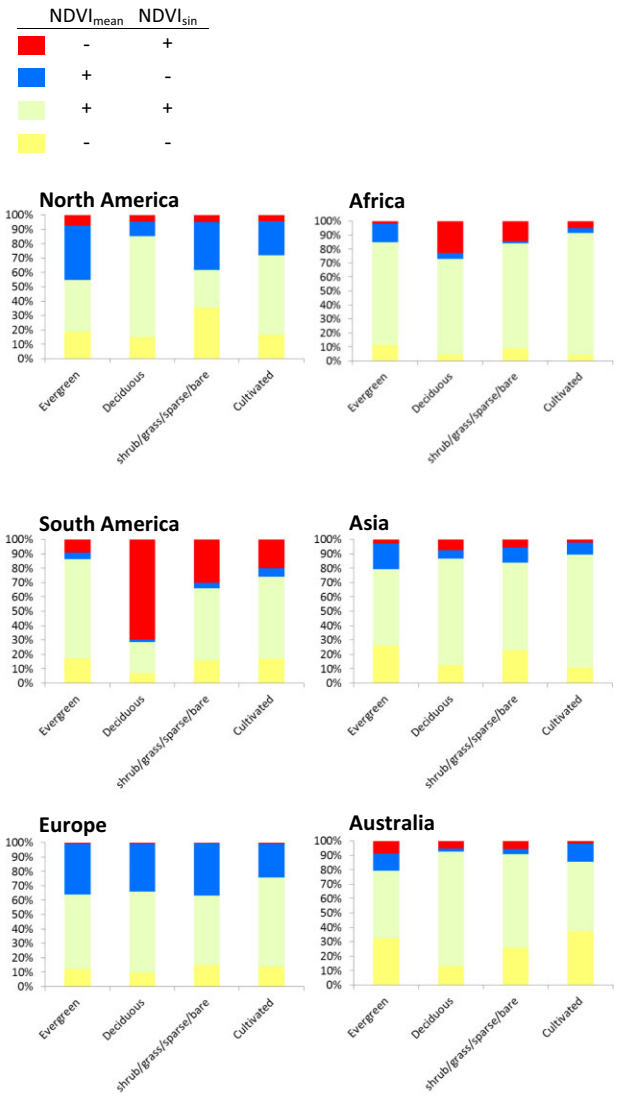

Figure 5 Distribution of pixels (in per cent) between categories of which both vegetation greenness metrics are characterized by a significant trend (positive/negative) (a–d in Table S1) plotted per continent and ecosystem functional type.

NDVI metric trend intercomparison

A direct comparison of trends from $NDVI_{mean}$ and $NDVI_{SIN}$ (Fig. 2) is made for the common denominator of non-masked pixels in Fig. 1(a) and (b) ($n = 833{,}863$). Considerably larger areas of pixels with positive trends in both NDVI metrics (pale green) (17.1%) are observed as compared to pixels with negative trends (pale yellow) (3.7%). Some 2.4% of the pixels are characterized by positive trends in $NDVI_{mean}$ and negative trends in $NDVI_{SIN}$ (blue), whereas the opposite pattern of negative trends in $NDVI_{mean}$ and positive trends in $NDVI_{SIN}$ (red) applies to 2.8% of the pixels. Large areas of consistent positive trends can be observed in the Sahelian and Sudano-Sahelian regions, India and eastern China, and more scattered clusters in central and north-east USA, southern Africa and Australia. Areas of consistent negative trends are generally much more scattered compared with the other three trend combinations, but clusters can be seen in northern Kenya, along the border between Kazakhstan and Uzbekistan and in north-east China.

When comparing patterns of trend differences (Fig. 2) with global land-cover classes aggregated into major categories of EFTs (Fig. S2) it can be seen that areas of negative trends in $NDVI_{mean}$ and positive trends in $NDVI_{SIN}$ (red, Fig. 2) for some areas coincide with the aggregated land-cover class of deciduous tree cover (light green, Fig. S2), whereas areas of positive trends in $NDVI_{mean}$ and negative trends in $NDVI_{SIN}$ (blue, Fig. 2) are often associated with the presence of evergreen forest (dark green, Fig. S2) or cultivated areas (orange, Fig. S2).

The low ratio (Table 1, Ratio a/b) between consistent (both NDVI metrics) negative and positive trends indicates that considerably more pixels are characterized by a consistent positive trend compared with negative trends for the majority of land-cover classes (GLC2000), with land-cover classes of limited/sparse vegetation (classes 14 and 19) having the highest ratios. The relation between pixels of opposite NDVI metric trends and land-cover classes supports the spatial concurrence of the maps in Figs 2 & S2. Larger percentage values of the combination of positive $NDVI_{mean}$ trends and negative $NDVI_{SIN}$ trends ('diverging trends case 1', Table S1) as compared with negative $NDVI_{mean}$/positive $NDVI_{SIN}$ trends ('diverging trends case 2', Table S1; indicated by the ratio $c/d > 1$) are observed for the evergreen tree-cover classes 1, 4 and 6 (and also class 17, which is a mixture of cropland and tree cover). For the three classes of deciduous tree cover (2, 3 and 5) a distinctly different pattern is observed with a predominance of 'diverging trends case 2' (ratio $c/d < 1$). The same pattern of diverging trends between evergreen and deciduous vegetation is found for the two classes of shrub cover (classes 11 and 12) with shrub cover, evergreen, showing a ratio of 3.88 and shrub cover, deciduous, a ratio of 0.53.

Diverging NDVI metric trends per EFT

An analysis of pixels of diverging trends for the two NDVI metrics was conducted at the global scale for land-cover classes that were aggregated into major EFT categories (as indicated by the colouring of classes in Fig. S2). Results are calculated as the percentage of the total number of pixels within the 'diverging trends cases 1 and 2' classes for each EFT and the number of pixel counts is given in parentheses to indicate the spatial extent of classes for the individual EFTs (Fig. 3). The percentage of pixels belonging to the 'diverging trends case 1' class (blue bars) is higher than for the 'diverging trends case 2' (red bars) for cultivated areas whereas the opposite (more pixels of the 'diverging trends case 2' class) is predominant for the three remaining EFTs (flooded vegetation, however, only covers a limited number of pixels). The EFT of tree cover has been further divided into subcategories of evergreen and deciduous (Fig. 3, right part). This subdivision reveals that a considerably higher proportion of pixels of deciduous forest are characterized by

Table 1 NDVI trend combination when combining $NDVI_{mean}$ and $NDVI_{SIN}$ time series trends (a–g in Table S1; the first mentioned trend represents $NDVI_{mean}$ and the second trend, $NDVI_{SIN}$) per GLC2000 land-cover class.

	$NDVI_{mean}$–$NDVI_{SIN}$ trend combinations								
Land-cover classes (GLC2000)	(a) Negative–negative	(b) Positive–positive	Ratio a/b	(c) Positive–negative	(d) Negative–positive	Ratio c/d	(e) Not sig.–not sig.	(f) Not sig.–pos./neg.	(g) Pos./neg.–not sig.
(1) Tree cover, broadleaved, evergreen	(%) 4.67	13.48	0.35	1.93	1.66	1.16	31.87	15.22	31.17
	(*n*) 3732	10,769		1539	1325		25,451	12,152	24,892
(2) Tree cover, broadleaved, deciduous, closed	2.93	15.73	0.19	2.11	8.81	0.24	22.88	28.77	18.76
	1,444	7,743		1040	4338		11,259	14,157	9231
(3) Tree cover, broadleaved, deciduous, open	1.89	24.85	0.08	1.41	5.33	0.27	19.02	31.59	15.90
	835	11,000		626	2359		8,420	13,984	7,040
(4) Tree cover, needle-leaved, evergreen	4.50	11.48	0.39	8.27	1.02	8.13	28.42	14.96	31.36
	1366	3488		2513	309		8636	4547	9528
(5) Tree cover, needle-leaved, deciduous	1.46	11.04	0.13	1.04	14.38	0.07	10.83	51.88	9.38
	7	53		5	69		52	249	45
(6) Tree cover, mixed leaf type	4.15	18.40	0.23	6.13	0.79	7.78	19.47	11.91	39.15
	195	864		288	37		914	559	1838
(7) Tree cover, regularly flooded, fresh water	3.69	13.49	0.27	1.91	0.77	2.46	33.27	11.92	34.94
	124	453		64	26		1117	400	1173
(8) Tree cover, regularly flooded, saline water	5.12	13.14	0.39	1.19	2.47	0.48	31.48	17.41	29.18
	60	154		14	29		369	204	342
(9) Mosaic: tree cover/other natural vegetation	2.50	29.37	0.09	4.63	0.21	22.50	16.45	6.07	40.77
	194	2282		360	16		1278	472	3168
(10) Tree cover, burnt	7.81	17.19	0.45	3.13	0.00	–	37.50	21.88	12.50
	5	11		2	0		24	14	8
(11) Shrub cover, closed-open, evergreen	4.83	12.87	0.38	2.64	0.68	3.88	35.64	17.17	26.17
	510	1358		279	72		3761	1812	2762
(12) Shrub cover, closed-open, deciduous	2.92	18.92	0.15	1.64	3.11	0.53	30.77	27.11	15.54
	3033	19,617		1705	3220		31,905	28,109	16,112
(13) Herbaceous cover, closed-open	3.90	12.17	0.32	2.07	2.04	1.01	37.15	26.01	16.65
	4478	13,980		2382	2349		42,690	29,893	19,136
(14) Sparse herbaceous or sparse shrub cover	4.29	8.50	0.50	0.80	4.09	0.20	42.21	24.57	15.55
	2768	5491		515	2640		27,260	15,865	10,044
(15) Regularly flooded shrub and/or herbaceous cover	3.66	13.20	0.28	1.27	4.22	0.30	32.06	25.70	19.90
	268	967		93	309		2349	1883	1458
(16) Cultivated and managed areas	3.45	23.12	0.15	2.89	1.62	1.78	24.50	19.52	24.91
	5523	36,983		4619	2590		39,192	31,217	39,839
(17) Mosaic: cropland/tree cover/other natural vegetation	4.67	11.26	0.41	4.51	1.39	3.24	27.86	12.67	37.64
	1145	2763		1107	342		6837	3109	9235
(18) Mosaic: cropland/shrub and/or grass cover	2.43	36.53	0.07	1.96	3.06	0.64	19.65	21.40	14.97
	647	9714		522	813		5226	5691	3982
(19) Bare areas	6.81	7.58	0.90	1.32	2.82	0.47	40.51	19.08	21.88
	1486	1655		288	615		8839	4163	4774

The first row in a cell is the number of pixels in per cent per land-cover class belonging to a given trend combination and second row is the total number of observations per land-cover class belonging to a given trend combination.

'diverging trends case 2' whereas the opposite combination ('diverging trends case 1') dominates for evergreen tree cover.

To study what inter- and intra-annual patterns of change in NDVI are causing diverging trends in NDVI metrics ('diverging trends cases 1 and 2' in Table S1), the original 15-day composite GIMMS3g NDVI time series, averaged for pixels of different land-cover classes (selected from the analyses presented in Fig. 3), are shown in Fig. 4. The majority of pixels of diverging trends for the EFT categories covering GLC2000 land-cover classes of tree cover deciduous and shrub/herbaceous/sparse/bare (light green and yellow in Fig. S2) are characterized by 'diverging trends case 2' (Table S1). NDVI time series of the individual GLC2000 land-cover classes (Fig. 4, top) of tree cover, broadleaved, deciduous, open (class 3, Fig. S2) and shrub cover, closed–open, deciduous (class 12, Fig. S2) are deciduous vegetation, but belong to different EFTs. In both cases the diverging trends in NDVI metrics stem from NDVI time series showing lower values for non-growing period over the last decade (from 2001), whereas the maximum NDVI during growing the season remains stable. This change pattern produces decreased values of $NDVI_{mean}$ whereas the lower non-growing period values cause an increase in $NDVI_{SIN}$ because of the larger amplitude between the maximum and minimum values (the calculation of $NDVI_{SIN}$ is based on a percentage of the amplitude). The majority of pixels of diverging trends for the EFT categories tree cover evergreen and cultivated [classes 1, 4 and 6 (dark green) and 16–18 (orange) in Fig. S2] are characterized by 'diverging trends case 1' (Table S1). NDVI time series (Fig. 4, bottom) for three GLC2000 land-cover classes [tree cover evergreen (1), cropland (16), mixed (17)] all show the same temporal pattern of an increased non-growing period NDVI level compared with a more stable growing season maximum value producing positive $NDVI_{mean}$ trends and negative $NDVI_{SIN}$ trends.

Analysis per continent

An analysis of the different NDVI metric trends for EFTs of tree cover evergreen, tree cover deciduous, shrub/herbaceous/sparse/bare and cultivated areas was conducted per continent. Pixels characterized by both time series of NDVI metrics being significant (either positive or negative; categories a–d in Table S1) and pixels where at least one NDVI metric is significant (either positive or negative; categories e and f in Table S1) are tabulated in Table 2. The highest concentrations of pixels (in %) with a significant trend (both metrics, categories a–d, and for at least one metric, categories e and f) are found in Europe and Africa, while the lowest concentrations are found in Australia. When the EFTs are separated, the highest concentrations of pixels for which both time series of NDVI metrics are significant are predominantly found for EFTs of deciduous tree cover and cultivated areas (except for South America, where cultivated areas have the lowest percentage value). The EFT of deciduous is ranked first (highest percentage cover of significant trends) in four out of six continents (Table 2) and agriculture is ranked first two out of six times (Africa and Asia) and second three times (North America, Europe, Australia).

For pixels for which both NDVI metrics are characterized by a significant trend (column 5, Table 2), distributions between categories (a–d in Table S1) are plotted per continent and EFT (Fig. 5). It is clear that, for most continents, the majority of pixels are characterized by converging trends of positive NDVI metrics. However, for South America the largest number of pixels are characterized by 'diverging trends case 2' (category d) for deciduous tree cover, and for North America 'diverging trends case 1' (category c) describes most of the evergreen tree-cover pixels. For both Europe and North America there are much higher numbers of pixels of 'diverging trends case 1' for all EFTs compared with the 'diverging trends case 2' (less pronounced for North America deciduous tree cover). In South America the opposite is observed, with much higher numbers of 'diverging trends case 2' for all EFTs (especially deciduous tree cover). In Africa, Asia and Australia, the proportions of pixels of diverging NDVI metric trends are smaller, yet there is a tendency for more pixels that are classified as deciduous tree cover to be characterized by 'diverging trends case 2' compared with 'diverging trends case 1'.

DISCUSSION

Relating diverging trends to changes in LULCC

This study shows how information on large-scale changes in ecosystem functioning over the last three decades can be derived from the GIMMS3g NDVI dataset. By combining different methods for vegetation parameterization with different sensitivity to the persistent and recurrent vegetation components we have shown that structural attributes of ecosystems related to the changes in ecosystem functioning (here monitored as changes in the composition of EFTs) can be extracted at regional to global scales. The global trend maps of 30-year time series of the different NDVI metrics are similar for the majority of land areas but areas of diverging NDVI metric trends ($NDVI_{mean}$ and $NDVI_{SIN}$) are predominant for EFTs of deciduous tree cover. The observed changes in ecosystem functioning can be coupled to LULCC at the regional scale, but the specific type and drivers of LULCC might be very different from region to region.

Diverging trends and changes in tree cover

From the global map of converging/diverging trends of the NDVI metrics, areas of negative trends in $NDVI_{mean}$ and positive trends in $NDVI_{SIN}$ ('diverging trends case 2' in Table S1 and red in Fig. 2) are shown to dominate for land-cover classes of deciduous forest in tropical and subtropical areas. Diverging trends in deciduous forests in these areas are hypothesized to be caused by changes in the ratio of persistent/recurrent vegetation, and time series of 15-day composite GIMMS3g NDVI data reveal that the diverging trends in these ecosystems can be explained by temporal changes in the ratio of non-growing period/growing season NDVI integrals. For areas characterized by a decreasing non-growing period NDVI and a constant maximum growing season NDVI (Fig. 4, top), this will inevi-

Table 2 Statistics of time series trend combinations for the $NDVI_{mean}$ and $NDVI_{SIN}$ metrics grouped per continent (cont.) and as a function of ecosystem functional types. Statistics exclude pixels masked as non-vegetated, dense forest or snow covered.

				Both NDVI metrics significant (either positive or negative)				At least one NDVI metric significant (either positive or negative)			
Continent	Number of pixels	All pixels	All pixels cont. sum	*n*	Cont. sum	%	Cont. average	*n*	Cont. sum	%	Cont. average
North America	Evergreen tree cover	20,639	79,237	4992	17,032	24.2	23.8	14,148	50,807	68.6	67.9
	Deciduous tree cover	8668		2603		30.0		6710		77.4	
	Shrub/grass/sparse/bare	33,325		5248		15.7		18,073		54.2	
	Cultivated areas	16,605		4189		25.2		11,876		71.5	
South America	Evergreen tree cover	42,051	142,851	10,785	33,945	25.6	25.4	30,689	99,307	73.0	70.5
	Deciduous tree cover	12,619		4124		32.7		9451		74.9	
	Shrub/grass/sparse/bare	44,463		9870		22.2		29,815		67.1	
	Cultivated areas	43,718		9166		21.0		29,352		67.1	
Europe	Evergreen tree cover	3708	34,037	1162	11,106	31.3	32.9	3182	28,827	85.8	86.0
	Deciduous tree cover	3651		1382		37.9		3247		88.9	
	Shrub/grass/sparse/bare	6137		1808		29.5		5253		85.6	
	Cultivated areas	20,541		6754		32.9		17,145		83.5	
Africa	Evergreen tree cover	15,383	206,753	4467	64,946	29.0	32.3	12,531	160,280	81.5	79.8
	Deciduous tree cover	47,459		15,300		32.2		39,126		82.4	
	Shrub/grass/sparse/bare	97,070		25,672		26.4		69,400		71.5	
	Cultivated areas	46,841		19,507		41.6		39,223		83.7	
Asia	Evergreen tree cover	28,810	179,064	5748	50,116	20.0	27.3	18,175	124,724	63.1	69.3
	Deciduous tree cover	13,653		4105		30.1		9885		72.4	
	Shrub/grass/sparse/bare	68,300		16,256		23.8		43,555		63.8	
	Cultivated areas	68,301		24,007		35.1		53,109		77.8	
Australia	Evergreen tree cover	3569	70,875	478	11,164	13.4	16.7	2026	39,601	56.8	59.0
	Deciduous tree cover	6721		1431		21.3		4750		70.7	
	Shrub/grass/sparse/bare	52,598		7909		15.0		28,506		54.2	
	Cultivated areas	7987		1346		16.9		4319		54.1	

tably lead to a divergence in the two NDVI metrics ($NDVI_{mean}$ and $NDVI_{SIN}$). These in turn are likely to show areas of significant change in tree cover (tree cover being the only source of influence on the non-growing period NDVI). For a successful decomposition of persistent and recurrent vegetation, the phenological cycle of the two needs to be separable in time. This is typical for those biomes in which the dominant woody vegetation is evergreen and the dominant herbaceous vegetation consists of annual grasses, crops and pastures. Also, for deciduous forest in tropical and subtropical areas (Fig. S2), the vegetative/senescent stages of woody and herbaceous cover are often different. Typically, the trees shed their leaves for a short time in the non-growing period to reduce water loss (this varies with species type) and produce a flush of new leaves before the onset of the rainy season. The greening of the woody cover thereby precedes the herbaceous vegetation cycle that is controlled to a higher degree by the onset of the rainy season. In a recent study by Mitchard & Flintrop (2013), forest degradation in the dry deciduous forest of Africa was assessed with an earlier version of the GIMMS NDVI using information from the dry season only. Lu *et al.* (2003) used an AVHRR NDVI time series to decompose contributions from woody (perennial) and herbaceous (annual) vegetation to infer their separate leaf area indices and cover fractions for Australia using time series decomposition techniques.

The pronounced pattern of diverging NDVI trends in central South America (covering parts of Bolivia, Paraguay and northern Argentina) coincides with the areal extent of the dry Chaco region (Portillo-Quintero & Sanchez-Azofeifa, 2010). The dry Chaco is known as one of the most active deforestation frontiers of South American dry forest in recent decades because of the agricultural expansion of soybean production. Deforestation rates increased during the 1980s and 1990s, driven by the sustained global demand for soybeans, and were accelerated between 2001 and 2007 following the global increase in commodity prices (Gasparri & Grau, 2009; who used Landsat imagery to assess the deforestation rates in subsets of the dry Chaco region). The explanation of this pattern ('diverging trends case 2') as being related to a loss in tree cover corresponds well to Clark *et al.* (2012), who found the second largest hotspot of deforestation in Central and South America to be in the drought-deciduous, dry forests of Argentina, Paraguay and Bolivia, with a loss of 125,867 km^2 of closed-canopy forest and gains of 41,292 and 82,674 km^2 in open-canopy forests and agriculture and pastures, respectively (assessed from 250-m MODIS imagery covering 2001–10). The present study, however, synthesizes 'wall-to-wall' changes in the tropical dry forest covering a period of three decades (1982–2011) and can therefore be used to analyse longer temporal scales than newer generations of EO-based datasets from sensors like MODIS (2000–present), SPOT VGT (1998–2014) and MERIS (2002–12) would have allowed.

The belt of diverging NDVI trends ('diverging trends case 2'; red, Fig. 2) across south-central Africa (Angola, Zambia, Tanzania, and Mozambique) corresponds to the extent of Miombo woodlands (White, 1983). Forest degradation is an important cause of loss of wood biomass in Miombo woodland (Chidumayo, 2013) and is by definition more challenging to monitor using EO data than deforestation because of the subtle changes in tree cover over time (Joseph *et al.*, 2011). Forest degradation in the Miombo woodlands was assessed by Mitchard & Flintrop (2013), and the results of potential forest degradation match well the south-central Africa pixels of diverging trends in Fig. 2. However, new information on the drivers of observed change is provided in the current study since the recurrent vegetation is not observed to decline during the growing season; this does not suggest climate-induced degradation but rather human-induced forest degradation.

The pronounced area of diverging NDVI trends ('diverging trends case 2'; red, Fig. 2) in the central Sahel covers southern Niger (the Fakara region). The area consists of highly fragmented agro-pastoral land with a dynamic land use and is characterized by a large increase in land area under cultivation that has occurred over the last decades (Dardel *et al.*, 2014) and has resulted in a decrease in shrub/tree cover.

Woody encroachment in sub-Saharan African woodlands and savannas (south of Sahel) has also been reported. Mitchard & Flintrop (2013) conducted a literature review from across Africa's savannas and woodlands where woody encroachment was found to dominate. The sub-Saharan areas of diverging trends ('diverging trends case 1') for deciduous tree cover driven by increasing values in dry season NDVI values (blue, Fig. 2) correspond to areas of reported woody encroachment in Cameroon as based on optical and radar remote sensing (Mitchard *et al.*, 2009, 2011). Areas of diverging trends ('diverging trends case 1') caused by an increase in dry season NDVI are also found in Ivory Coast/southern Ghana. A multi-scale approach comprising combined household survey research on environmental perceptions with aerial photo interpretation and vegetation transects was conducted in the Ivory Coast by Bassett & Zueli (2000) to identify the general trends in vegetation change. Farmers and herders reported more wooded landscapes, which coincided with the aerial image interpretation for the region.

The predominance of pixels characterized by 'diverging trends case 1' for evergreen forest in North America (Fig. 5) is caused by an increase in non-growing period (winter) NDVI without a corresponding increase in growing season NDVI during recent decades. The majority of 'diverging trends case 1' pixels observed in the south-eastern USA covered by the evergreen forest class belong to needle-leaved forest (note, however, that the majority of pixels classified as needle-leaved forest in boreal/arctic areas of both continents have been masked out due to the influence from snow cover). This corresponds well to the results of Wear & Greis (2012), who reported a doubling of evergreen forest (pine timber production) in south-eastern USA over the last 40 years.

Diverging trends and changes in agricultural practice

Diverging trends in cultivated areas are likely to be caused by changes in agricultural practices. In both western Europe and

south-eastern USA (major parts of eastern/northern Europe and northern/western USA are masked due to the influence of snow cover), substantial regions classified as agriculture (Fig. S2) are characterized by diverging trends ('diverging trends case 1'; blue, Fig. 2) caused by an increase in winter NDVI (Fig. 4, bottom). This has probably been caused by changes in agricultural practice during the period 1982–2011. For western Europe, winter crops include primarily wheat and secondarily barley (FAOSTAT, 2014), and according to Olesen & Bindi (2002) wheat yield trends in north-western Europe (the UK and France) have increased rapidly over the past three decades (60% increase in yield production). Increasing yields can be due to agricultural expansion and/or intensification; both are likely to influence the winter period NDVI signal. There was a 28% expansion in the wheat area harvested in western Europe between 1982 and 2011 (FAOSTAT, 2014), which corresponds well with the spatial patterns found for Europe in Fig. 2. In central and south-eastern USA, winter cereals consist also primarily of wheat (soft and hard red winter wheat), but despite an increase in yield of 23% (FAOSTAT, 2014 entire USA) the harvested area decreased throughout the period studied (−41%, entire USA). However, 'fodder temporary' and 'pasture permanent' are winter crops not included in FAOSTAT that, according to different FAO statistics, together cover an area of the same size as winter wheat in south-eastern USA and an area three times larger than winter wheat in central USA (AQUASTAT, 2012). Therefore, the relationship between winter greening and changes in LULCC in central and south-eastern USA based on FAO statistics is inconclusive. An increase in late autumn and winter NDVI was found by Tsai *et al.* (2014) in the state of Florida over the period 1982–2006 and was suggested to be caused by changes in the Atlantic multi-decadal oscillation (AMO), which switched from a cold to a warm phase after 1995 and is associated with increased winter precipitation.

ACKNOWLEDGEMENTS

The authors thank NASA GIMMS Group for producing and sharing the GIMMS3g NDVI dataset. NASA/MODIS Land Discipline Group is thanked for sharing the MODIS LAND data. The team behind the GLC2000 land-cover data is thanked for producing and sharing the data. Finally, P. Jonsson, Center for Technology Studies, Malmö University and L. Eklundh, Department of Physical Geography and Ecosystem Science, Lund University are thanked for sharing the TIMESAT software. This research is part of the project entitled 'Earth observation-based vegetation productivity and land degradation trends in global drylands'. The project is funded by the Danish Council for Independent Research (DFF) Sapere Aude programme.

REFERENCES

Alcaraz-Segura, D., Paruelo, J. & Cabello, J. (2006) Identification of current ecosystem functional types in the Iberian Peninsula. *Global Ecology and Biogeography*, **15**, 200–212.

An, Y.Z., Gao, W. & Gao, Z.Q. (2014) Characterizing land condition variability in northern China from 1982 to 2011. *Environmental Earth Sciences*, **72**, 663–676.

AQUASTAT (2012) Irrigation water requirement and water withdrawal by country. Available at: http://www.fao.org/nr/water/aquastat/water_use_agr/index.stm.

Asner, G.P., Knapp, D.E., Balaji, A. & Paez-Acosta, G. (2009) Automated mapping of tropical deforestation and forest degradation: CLASlite. *Journal of Applied Remote Sensing*, **3**, 033543.

Bartholomé, E., Belward, A.S., Achard, F., Bartalev, S., Carmona-Moreno, C., Eva, H., Fritz, S., Gregoire, J.-M., Mayaux, P., Stibig, H.-J.E.E. & European Commission, Luxembourg (2002) *Global land cover mapping for the year 2000 – project status November 2002*. EUR 20524. European Commission, Luxembourg.

Bassett, T.J. & Zueli, K.B. (2000) Environmental discourses and the Ivorian savanna. *Annals of the Association of American Geographers*, **90**, 67–95.

de Beurs, K.M. & Henebry, G.M. (2005) Land surface phenology and temperature variation in the International Geosphere–Biosphere Program high-latitude transects. *Global Change Biology*, **11**, 779–790.

Chidumayo, E.N. (2013) Forest degradation and recovery in a Miombo woodland landscape in Zambia: 22 years of observations on permanent sample plots. *Forest Ecology and Management*, **291**, 154–161.

Clark, M.L., Aide, T.M. & Riner, G. (2012) Land change for all municipalities in Latin America and the Caribbean assessed from 250-m MODIS imagery (2001–2010). *Remote Sensing of Environment*, **126**, 84–103.

Dardel, C., Kergoat, L., Hiernaux, P., Mougin, E., Grippa, M. & Tucker, C.J. (2014) Re-greening Sahel: 30 years of remote sensing data and field observations (Mali, Niger). *Remote Sensing of Environment*, **140**, 350–364.

Di Gregorio, A. & Jansen, L. (2000) *Land cover classification system, classification concepts and user manual*. Food and Agriculture Organization of the United Nations, Rome.

Donohue, R.J., McVicar, T.R. & Roderick, M.L. (2009) Climate-related trends in Australian vegetation cover as inferred from satellite observations, 1981–2006. *Global Change Biology*, **15**, 1025–1039.

Eastman, J.R., Sangermano, F., Ghimire, B., Zhu, H.L., Chen, H., Neeti, N., Cai, Y.M., Machado, E.A. & Crema, S.C. (2009) Seasonal trend analysis of image time series. *International Journal of Remote Sensing*, **30**, 2721–2726.

FAOSTAT (2014) FAOSTAT. Available at: http://faostat.fao.org/site/567/default.aspx#ancor (accessed 2014).

Fensholt, R. & Proud, S.R. (2012) Evaluation of Earth observation based global long term vegetation trends – comparing GIMMS and MODIS global NDVI time series. *Remote Sensing of Environment*, **119**, 131–147.

Fensholt, R., Langanke, T., Rasmussen, K., Reenberg, A., Prince, S.D., Tucker, C., Scholes, R.J., Le, Q.B., Bondeau, A., Eastman, R., Epstein, H., Gaughan, A.E., Hellden, U., Mbow, C., Olsson, L., Paruelo, J., Schweitzer, C., Seaquist, J. &

Wessels, K. (2012) Greenness in semi-arid areas across the globe 1981–2007 – an earth observing satellite based analysis of trends and drivers. *Remote Sensing of Environment*, **121**, 144–158.

Fensholt, R., Rasmussen, K., Kaspersen, P., Huber, S., Horion, S. & Swinnen, E. (2013) Assessing land degradation/recovery in the African Sahel from long-term earth observation based primary productivity and precipitation relationships. *Remote Sensing*, **5**, 664–686.

Gasparri, N.I. & Grau, H.R. (2009) Deforestation and fragmentation of Chaco dry forest in NW Argentina (1972–2007). *Forest Ecology and Management*, **258**, 913–921.

Hansen, M.C., Potapov, P.V., Moore, R., Hancher, M., Turubanova, S.A., Tyukavina, A., Thau, D., Stehman, S.V., Goetz, S.J., Loveland, T.R., Kommareddy, A., Egorov, A., Chini, L., Justice, C.O. & Townshend, J.R.G. (2013) High-resolution global maps of 21st-century forest cover change. *Science*, **342**, 850–853.

Hirsch, R.M. & Slack, J.R. (1984) A nonparametric trend test for seasonal data with serial dependence. *Water Resources Research*, **20**, 727–732.

Hoaglin, D.C., Mosteller, F. & Tukey, J.W. (2000) *Understanding robust and exploratory data analysis*. Wiley, New York.

Ivits, E., Cherlet, M., Horion, S. & Fensholt, R. (2013) Global biogeographical pattern of ecosystem functional types derived from earth observation data. *Remote Sensing*, **5**, 3305–3330.

Ivits, E., Horion, S., Fensholt, R. & Cherlet, M. (2014) Global ecosystem response types derived from the standardized precipitation evapotranspiration index and FPAR3g series. *Remote Sensing*, **6**, 4266–4288.

de Jong, R., de Bruin, S., de Wit, A., Schaepman, M.E. & Dent, D.L. (2011) Analysis of monotonic greening and browning trends from global NDVI time-series. *Remote Sensing of Environment*, **115**, 692–702.

Jonsson, P. & Eklundh, L. (2002) Seasonality extraction by function fitting to time-series of satellite sensor data. *IEEE Transactions on Geoscience and Remote Sensing*, **40**, 1824–1832.

Jonsson, P. & Eklundh, L. (2004) TIMESAT – a program for analyzing time-series of satellite sensor data. *Computers and Geosciences*, **30**, 833–845.

Joseph, S., Murthy, M.S.R. & Thomas, A.P. (2011) The progress on remote sensing technology in identifying tropical forest degradation: a synthesis of the present knowledge and future perspectives. *Environmental Earth Sciences*, **64**, 731–741.

Lambin, E.F. (1999) Monitoring forest degradation in tropical regions by remote sensing: some methodological issues. *Global Ecology and Biogeography*, **8**, 191–198.

van Leeuwen, W.J.D., Hartfield, K., Miranda, M. & Meza, F.J. (2013) Trends and ENSO/AAO driven variability in NDVI derived productivity and phenology alongside the Andes mountains. *Remote Sensing*, **5**, 1177–1203.

Lu, H., Raupach, M.R., McVicar, T.R. & Barrett, D.J. (2003) Decomposition of vegetation cover into woody and herbaceous components using AVHRR NDVI time series. *Remote Sensing of Environment*, **86**, 1–18.

Mitchard, E.T.A. & Flintrop, C.M. (2013) Woody encroachment and forest degradation in sub-Saharan Africa's woodlands and savannas 1982–2006. *Philosophical Transactions of the Royal Society B: Biological Sciences*, **368**, 20120406.

Mitchard, E.T.A., Saatchi, S.S., Gerard, F.F., Lewis, S.L. & Meir, P. (2009) Measuring woody encroachment along a forest–savanna boundary in central Africa. *Earth Interactions*, **13**, 1–19.

Mitchard, E.T.A., Saatchi, S.S., Lewis, S.L., Feldpausch, T.R., Woodhouse, I.H., Sonke, B., Rowland, C. & Meir, P. (2011) Measuring biomass changes due to woody encroachment and deforestation/degradation in a forest–savanna boundary region of central Africa using multi-temporal L-band radar backscatter. *Remote Sensing of Environment*, **115**, 2861–2873.

Myneni, R.B., Hall, F.G., Sellers, P.J. & Marshak, A.L. (1995) The interpretation of spectral vegetation indexes. *IEEE Transactions on Geoscience and Remote Sensing*, **33**, 481–486.

Nemani, R.R., Keeling, C.D., Hashimoto, H., Jolly, W.M., Piper, S.C., Tucker, C.J., Myneni, R.B. & Running, S.W. (2003) Climate-driven increases in global terrestrial net primary production from 1982 to 1999. *Science*, **300**, 1560–1563.

Olesen, J.E. & Bindi, M. (2002) Consequences of climate change for European agricultural productivity, land use and policy. *European Journal of Agronomy*, **16**, 239–262.

Paruelo, J.M., Jobbagy, E.G. & Sala, O.E. (2001) Current distribution of ecosystem functional types in temperate South America. *Ecosystems*, **4**, 683–698.

Piao, S.L., Mohammat, A., Fang, J.Y., Cai, Q. & Feng, J.M. (2006) NDVI-based increase in growth of temperate grasslands and its responses to climate changes in China. *Global Environmental Change – Human and Policy Dimensions*, **16**, 340–348.

Pinzon, J.E. & Tucker, C.J. (2014) A non-stationary 1981–2012 AVHRR NDVI3g time series. *Remote Sensing*, **6**, 6929–6960.

Portillo-Quintero, C.A. & Sanchez-Azofeifa, G.A. (2010) Extent and conservation of tropical dry forests in the Americas. *Biological Conservation*, **143**, 144–155.

Scholes, R.J., Pickett, G., Ellery, W.N. & Blackmore, A.C. (1997) Plant functional types in African savannas and grasslands. *Plant functional types: their relevance to ecosystem properties and global change* (ed. by T.M. Smith, H.H. Shugart and F.I. Woodward), pp. 255–268. Cambridge University Press, Cambridge.

Tsai, H.P., Southworth, J. & Waylen, P. (2014) Spatial persistence and temporal patterns in vegetation cover across Florida, 1982–2006. *Physical Geography*, **35**, 151–180.

Tucker, C.J. (1979) Red and photographic infrared linear combinations for monitoring vegetation. *Remote Sensing of Environment*, **8**, 127–150.

Wear, D.N. & Greis, J.G. (2012) *The Southern Forest Futures Project: summary report*. USDA Forest Service, Asheville, NC.

White, F. (1983) *The vegetation of Africa: a descriptive memoir to accompany the UNESCO/AETFAT/UNSO vegetation map of Africa*. UNESCO, Paris.

SUPPORTING INFORMATION

Additional supporting information may be found in the online version of this article at the publisher's web-site.

Figure S1 Amplitude and frequency changes for an idealized phenological curve representing the annual vegetation growth cycle.

Figure S2 Land-cover classes (GLC2000) merged into major ecosystem functional types of: tree cover deciduous, tree cover evergreen, tree cover flooded, shrub/sparse/bare and cropland.

Table S1 NDVI time series trend combinations when subtracting $NDVI_{mean}$ and $NDVI_{SIN}$ time series trends (significance criterion, $P < 0.1$).

BIOSKETCH

Rasmus Fensholt is an associate professor in earth observation ecology studies at the Department of Geosciences and Natural Resource Management, Section of Geography, University of Copenhagen. His research interests focus on remotely sensed assessment of biogeophysical variables related to terrestrial vegetation and changes in the global resource base of ecosystem services related to vegetation productivity.

Editor: Josep Peñuelas